TABLE I
SUMMARY OF PERFORMANCE COMPARISON

algorithms	time complexity	ROM space	special condition	modulo adder size
[2]	$O(\log n)$	$> n^2$	no	$n * M$
[4]	$O(\log n)$	$> n^2$	yes	2^k
[3]	$O(n)$	$O(n)$	no	M
New algorithm	$O(\log n)$	$O(n)$	no	$< M$

in the figure are the same. Each cell in the tree performs the findno algorithm. In the diagram, the RNS representation is used as input to the first level of cells in pair, i.e., $(x_1, x_2), (x_3, x_4), \cdots, (x_{n-1}, x_n)$. $\{P_i \mid i = 1, \cdots, n\}$ is the module set. They are also paired as inputs to the cells. At the first level, output $x_{ij}, j = i + 1$ is produced by the cell whose inputs are x_i, x_j, P_i, P_j, such that $x_i = x_{ij} \bmod P_i, x_j = x_{ij} \bmod P_j$ and $x_{ij} < P_{ij} = P_i * P_j$. Outputs from the first level of cells are fed to the cells in the second level. This pattern continues until there is only one output from the final level, which is the number we want to find.

From Fig. 2, it is easily seen that for a module set of size n, in first level of the tree, there are n cells, the second level has $\lceil n/2 \rceil$ cells, and so on. The tree is of height $\log_2 n$. Therefore the time delay to decode the RNS number $(x_1, \cdots, x_n)$ is of $\log_2 n$. Each cell is implemented to perform algorithm "findno". For findno (x_1, x_2, P_1, P_2, N), the value k_0 is an integer such that $k_0 * P_1 = 1 \bmod P_2$ and is stored in a ROM. For algorithm "translate", the value of $\prod_{i=k}^{j} P_i$ are also stored in a ROM. The total ROM area required is $n + n/2 + n/4 + \cdots + 1$, which is of $O(n)$, which is better than the $\Omega(n^2)$ ROM area needed in [2]. In addition, in the algorithm proposed here, the modulo M adder is used only in the last cell, all the other adders are modulo $P_i * \cdots * P_j$ which is less than the value $M = P_1 * \cdots * P_n$. This is to be compared to the $n * M$ modulo adders required in [2]. Section VI provides an overall performance comparison among different algorithms including the algorithm proposed in this brief.

V. PERFORMANCE COMPARSION

Previous approaches may require the use of large table look-up, like all the CRT-based approaches, or they may need large modulo $M = P_1 * \cdots * P_n$ adders. Some approaches may require time delay greater than $O(\log n)$. Some other approaches, e.g., the approach in [4], restrict the module set such that $P_i = 2^k$ for some i. The approach proposed in this brief attempts to avoid such difficulties. The algorithm achieves the fastest time $O(\log n)$, has the minimum table look-up $O(n)$, and makes no assumption on the module set. Moreover, the suggested implementation structure is very regular. A summary of performance comparison of a number of approaches is shown in Table I.

In Table I, under the column marked "modulo adder size," $n * M$ means there are n adders used and all of them are modulo M, 2^k means there is a modulo 2^k adder. "$< M$" means the adders used are modulo $P_i * \cdots * P_j < M$.

VI. CONCLUSION

This brief proposes a new and better algorithm for RNS-to-decimal decoding. It is based on the idea of recursively decomposing the module set into two parts. The time complexity of this algorithm is of $O(\log n)$. The ROM area used is of order $O(n)$. The minimum number of modulo $M = P_1 * \cdots * P_n$ adders are used. There is no assumption on the module set.

REFERENCES

[1] F. J. Taylor, "Residue arithmetic: A tutorial with examples," *IEEE Comput.*, vol. 17, pp. 50–62, May 1984.
[2] K. Elleithy and M. A. Bayoumi, "Fast and flexible architectures for RNS arithmetic decoding," *IEEE Trans. Circuits Syst.*, vol. 39, pp. 226–235, Apr. 1992.
[3] W. K. Jenkins, "Techniques for residue-to-analog conversion for residue-encoded digital filters," *IEEE Trans. Circuits Syst.*, vol. CAS-25, pp. 555–562, July 1978.
[4] T. V. Vu, "Efficient implementations of the Chinese reminder theorem for sign detection and residue decoding," *IEEE Trans. Comput.*, vol. C-34, pp. 646–651, July 1985.
[5] R. M. Capocelli and R. G. Carlo, "Efficient VLSI networks for converting an integer from binary system to residue number system and vice versa," *IEEE Trans. Circuits Syst.*, vol. 35, pp. 1425–1430, Nov. 1988.
[6] T. Cormen, C. Leiserson, and R. Rivest, *Introduction to Algorithms*. Cambridge, MA: The MIT Press, 1990.

Nonlinear Dynamics and Switching Time Bifurcations of a Thyristor Controlled Reactor Circuit

Rajesh Rajaraman, Ian Dobson, and Sasan G. Jalali

***Abstract*— We study a thyristor controlled reactor circuit used for static VAR control of utility electric power systems. The circuit exhibits switching times which jump or bifurcate as fold or transcritical bifurcations. We study the nonlinear dynamics of the circuit using a Poincaré map and demonstrate that the Poincaré map has discontinuities and is not invertible. The circuit has multiple attractors. Moreover, the basin boundary separating the basins of attraction intersects with the Poincaré map discontinuities. These novel properties illustrate some of the basic features of dynamical systems theory for thyristor switching circuits.**

Manuscript received June 28, 1995; revised December 28, 1995. This work was supported in part from a NSF Presidential Young Investigator Grant ECS-9157192 and EPRI Contracts RP8010-30, RP4000-29, RP8050-03, and WO8050-03. This paper was recommended by Associate Editor M. K. Kazimierczuk.

R. Rajaraman and I. Dobson are with the Electrical and Computer Engineering Department, University of Wisconsin, Madison, WI 53706 USA.
S. G. Jalali is with Siemens Energy and Automation, Atlanta, GA 30202 USA.

Publisher Item Identifier S 1057-7122(96)08342-0.

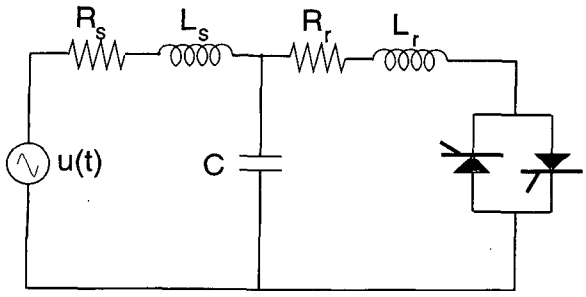

Fig. 1. Single phase static VAR system.

I. Introduction

As static switching circuits in large scale electric power systems proliferate, there is an increasing need to analyze and understand these circuits. Thyristor controlled reactors are used at the loaded ends of transmission lines to control the reactive power supplied from a fixed shunt capacitor so that voltage can be maintained when system loads or transmission line configurations change [6], [12], [10]. More recently, thyristor controlled reactors are emerging as one of the economical alternatives for flexible ac transmission (FACTS) [2], [7], [11]. This paper describes some basic aspects of nonlinear dynamics and bifurcations of a thyristor controlled reactor circuit. Thyristor controlled reactor circuits are a good choice for demonstrating the dynamics of switching circuits since they are both simple in form and exhibit interesting nonlinear behavior.

A key nonlinearity of a thyristor controlled reactor circuit is the dependence of the thyristor turn off time on the system state. For many initial conditions, the turn off time varies smoothly with changes in the initial condition and the behavior of the system is nonlinear but conventional. However, it is also possible for the switch off time to suddenly jump, or bifurcate. These switching time bifurcations can destabilize steady state circuit operation as circuit parameters slowly vary [8], [3], [9].

This brief addresses the different problem of fixing the circuit parameters and studying the effect of switching time bifurcations as the circuit initial conditions are varied. That is, the effect of switching time bifurcations on circuit transients is studied. The sudden jump in switch off times is described as a fold bifurcation and the onset of thyristor misfire is described as a transcritical bifurcation of switching times. We investigate the effects of the switching time bifurcations on the Poincaré map dynamics and phase portrait. The Poincaré map is shown to be noninvertible and discontinuous in some places and to have two asymptotically stable fixed points which correspond to asymptotically stable periodic orbits of the circuit. The boundary separating the basins of the two periodic orbits interacts with the Poincaré map discontinuities and has novel features. Some of these results first appeared in [13] and [14].

II. Circuit Description

Fig. 1 shows a single phase static VAR system [8], [1] consisting of a thyristor controlled reactor and a parallel capacitor $C = 1.5$ mF. The controlled reactor is modeled as an inductor $L_r = 1.66$ mH and resistor $R_r = 31.3$ mΩ in series. The static VAR system is connected to an infinite bus behind a power system impedance of inductance $L_s = 0.195$ mH and resistance $R_s = 0.9$ mΩ. The source voltage $u(t) = \sin(\omega t - 2\pi/3)$, where $\omega = 2\pi/T = 120\pi$ rad/s.

The switching element of the thyristor controlled reactor consists of two oppositely poled thyristors which conduct on alternate half cycles of the supply frequency. The thyristor is modeled as an ideal diode with a gate. The thyristor turns on when a firing pulse is applied at the gate, conducts current only in the forward direction, and turns off when the thyristor current becomes zero. The thyristor is a short circuit when on and an open circuit when off. These modeling assumptions are appropriate for systems studies of high power switching circuits. The phase delay of the thyristor firing is fixed at 120 degrees. One of the thyristors is fired at the beginning of the cycle ($t = 0$, T, 2T, $\cdots$) and the other thyristor is fired half way through the cycle ($t =$T/2, 3T/2, $\cdots$). The firing pulses are assumed to be very short.

When either of the thyristors conduct, the state vector $x(t) = (I_r(t), V_c(t), I_s(t))^t$ is specified by the thyristor controlled reactor current (kA), capacitor voltage (kV), and the source current (kA), and the system dynamics are

$$\dot{x} = Ax + Bu \tag{1}$$

where

$$A = \begin{pmatrix} -R_r L_r^{-1} & L_r^{-1} & 0 \\ -C^{-1} & 0 & C^{-1} \\ 0 & -L_s^{-1} & -R_s L_s^{-1} \end{pmatrix}; \quad B = \begin{pmatrix} 0 \\ 0 \\ L_s^{-1} \end{pmatrix}.$$

When both thyristors are off, the circuit state is constrained to lie in the plane $I_r = 0$ of zero thyristor current, the state vector $y(t) = (V_c(t), I_s(t))^t$ and the system dynamics are $\dot{y} = PAP^t y + PBu$ where

$$P = \begin{pmatrix} 0 & 1 & 0 \\ 0 & 0 & 1 \end{pmatrix}.$$

Further information on the circuit modeling is in [8].

III. Switching Conditions

We give switching conditions for the thyristor firing at $t = 0$; switching conditions for the thyristor firing at $t = T/2$ are similar. At time zero, the thyristor current $I_r(0) = 0$ and the initial state is given by $\lambda = y(0) = (V_c(0), I_s(0))^t$ or by $x(0) = (0, V_c(0), I_s(0))^t$. The function $f(t, \lambda)$ is defined to be the thyristor current assuming the thyristor is on for all time

$$f(t, \lambda) = (1\ 0\ 0)\left[e^{At}\begin{pmatrix} 0 \\ V_c(0) \\ I_s(0) \end{pmatrix} + \int_0^t e^{A(t-\tau)} Bu(\tau) d\tau\right].$$

Note that $f(0, \lambda) = 0$ for all λ.

The function $f(t, \lambda)$ can be used to describe the thyristor switching rules precisely. At $t = 0$, a thyristor is fired and will turn on unless a misfire occurs (a misfire occurs when the thyristor voltage, $V_c(0) < 0$). If there is no misfire and the thyristor switches on at $t = 0$, then the thyristor will switch off at the *first* positive root σ of f:

$$\sigma(\lambda) = \min\{\, t \mid f(t, \lambda) = 0,\ t > 0\}.$$

Note that, in contrast to diodes, thyristor switch on is inhibited until a firing pulse is present.

IV. Fold Bifurcation of Switching Times

The switching time σ for the thyristor firing at $t = 0$ is plotted as a function of the initial state $\lambda = y(0) = (V_c(0), I_s(0))^t$ in Fig. 2. Discontinuities of the switching time are apparent as sharp changes in the plot. These discontinuities can be understood by examining the roots of $f(t, \lambda)$. Fig. 3 shows a "slice" of Fig. 2 obtained by plotting several roots of $f(t, \lambda)$ versus the initial capacitor voltage $V_c(0)$ for a fixed initial source current $I_s(0) = 9$. The switching time σ is indicated by circles in the plot. As can be seen from Fig. 3, a discontinuity in the switching time occurs near $V_c(0) = 5.1$ where the first and second roots of $f(t, \lambda)$ coalesce and disappear so that

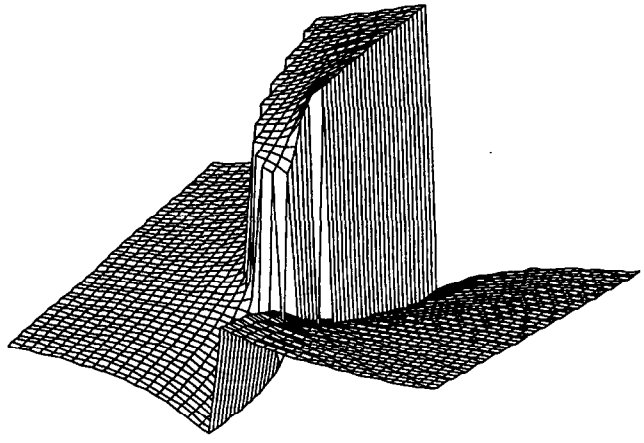

Fig. 2. 3-D plot of σ versus $\lambda = (V_c(0), I_s(0))$.

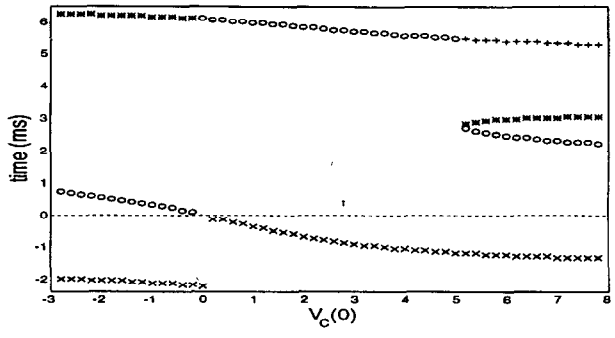

Fig. 3. Roots of $f(t,\lambda)$; $o = \sigma$, $* =$ root 2,$+$ =root 3,$\times$ = root$-$ $-$ 1, $--$ = root 0.

what was previously the third positive root becomes the first positive root and the switching time σ.

To analyze the discontinuity as a fold bifurcation of f, the thyristor is assumed to turn on with no misfire at $t = 0$ over the range of initial conditions λ of interest. It is proved in [3] that if the thyristor switch off at time $\sigma(\lambda_1)$ satisfies the transversality condition

$$\frac{\partial f}{\partial t}(\sigma(\lambda_1)) < 0$$

then $\sigma(\lambda)$ is a smooth function of λ for λ sufficiently near λ_1. If the thyristor switch off at time $\sigma(\lambda_*)$ does not satisfy the transversality condition, then the switch off time $\sigma(\lambda)$ is typically discontinuous at λ_*. For example, when $\lambda = \lambda_1 = (3.2, 4)^t$, the transversality condition is satisfied at the thyristor switch off at $\sigma(\lambda_1)$ as shown in Fig. 4(a). There is a second root of f near $\sigma(\lambda_1)$ and a third root of f at a later time. When $\lambda = \lambda_* = (4.2, 4)^t$ as in Fig. 4(b), f has zero gradient at the double root at $\sigma(\lambda_*)$ and the transversality condition is not satisfied. When λ changes to a new value $\lambda_2 = (5.2, 4)^t$ near λ_* as shown in Fig. 4(c), the previous first and second root have disappeared and the previous third root has suddenly become the first root.

V. Misfire Onset as a Transcritical Bifurcation

A thyristor misfires at a switch on time when the thyristor voltage is negative when the gate turn on pulse arrives. Consider the thyristor firing at $t = 0$ (the analysis is similar for misfire at $t = T/2$). Just before the gate pulse arrives, at time $t = 0-$, the thyristor voltage is the capacitor voltage $V_c(0)$ (see Fig. 1). From the system equations (1), $V_c(0)$ is proportional to $\frac{\partial f}{\partial t}(0, \lambda)$ which is the gradient of the thyristor current at $t = 0+$. Misfiring is described in the sequence

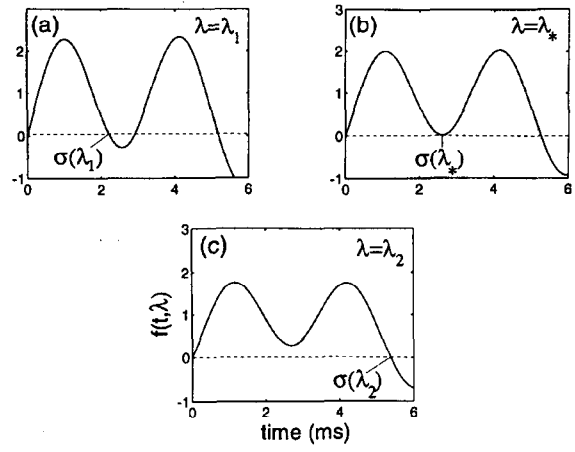

Fig. 4. $f(t,\lambda)$ versus t showing fold bifurcation.

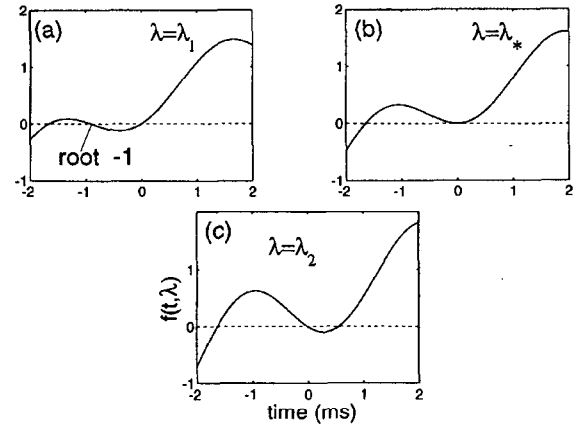

Fig. 5. $f(t,\lambda)$ versus t showing transcritical bifurcation.

of diagrams in Fig. 5(a)–(c) which are plots of $f(t,\lambda)$ versus t for various values of $V_c(0)$ with $I_s(0) = 4$. In Fig. 5(a) ($V_c(0) = 1$), the circuit is operating normally, and $\frac{\partial f}{\partial t}(0, \lambda_1) > 0$. In Fig. 5(b) ($V_c(0) = 0$), $\frac{\partial f}{\partial t}(0, \lambda_*)$ has decreased to zero and this is the onset of misfire. In Fig. 5(c) ($V_c(0) = -1$), the thyristor will misfire since $\frac{\partial f}{\partial t}(0, \lambda_2) < 0$. If we define root -1 to be the first negative root of $f(t,\lambda) = 0$, then root -1 increases through the root at zero and becomes relabeled as the first root when it becomes positive. The onset of the misfire occurs when root -1 coalesces with the root at zero. Since the root at zero is fixed, this is a transcritical bifurcation [5], [15] of roots of f. Also a transcritical bifurcation diagram is evident at the origin of Fig. 3.

Note that the onset of misfire for the thyristor firing at $t = 0$ can be predicted using $0 = \frac{\partial f}{\partial t}(0, \lambda) = [1\ 0\ 0]A(0\ V_c(0)\ I_s(0))^t$ which reduces to $V_c(0) = 0$. That is, the thyristor misfires for $V_c(0) < 0$. (If the system is in steady state with the initial condition λ on a periodic orbit such that $V_c(0)$ is near 0, then even a small change in parameters could cause a misfire to occur and the thyristor will not turn on; this sudden change in switching times will destabilize the system [9]. Note that, similarly to the case of fold bifurcation instabilities [3], the eigenvalues of the Jacobian of the Poincaré map give no warning of instability due to the onset of misfire.)

Interaction of the fold and transcritical bifurcations can be observed in Fig. 6(a)–(d). Each subplot is a bifurcation diagram showing the roots of $f(t,\lambda)$ versus $V_c(0)$ while holding $I_s(0)$ constant; the 4 subplots are obtained by varying $I_s(0)$. In Fig. 6(a) ($I_s(0) = 3.8$), there is a transcritical bifurcation at T, and no fold bifurcations.

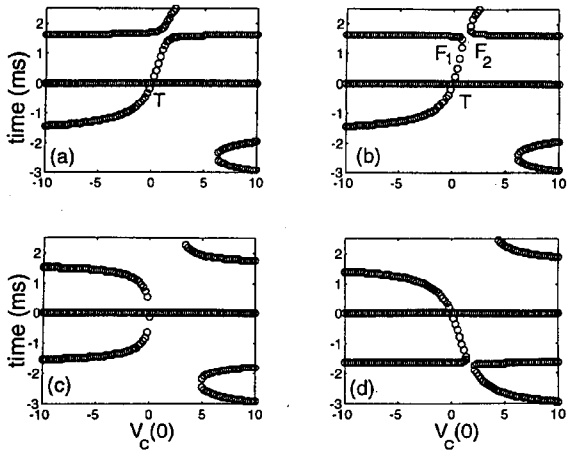

Fig. 6. Roots of $f(t, \lambda)$ showing bifurcations interacting.

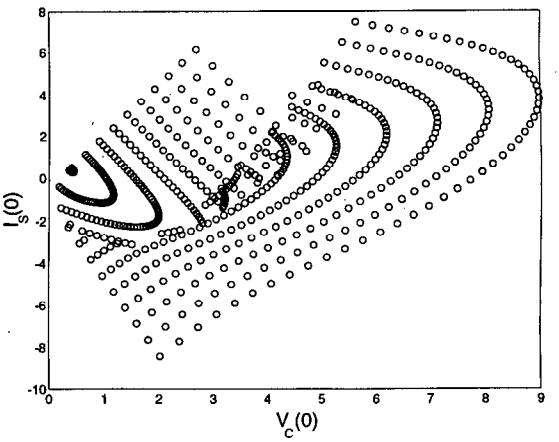

Fig. 7. Poincaré map of semidisk of radius 10.

We vary $I_s(0)$, and note that fold bifurcations F_1 and F_2 appear in Fig. 6(b) ($I_s(0) = 0.2$). As we continue varying $I_s(0)$, the bifurcations T and F_1 move closer and finally coalesce in Fig. 6(c) ($I_s(0) = -3$) to form a pitchfork bifurcation [5], [15]. The pitchfork bifurcation is not generic and as we continue to vary $I_s(0)$, the pitchfork bifurcation disappears, and in Fig. 6(d) ($I_s(0) = -3.4$) the generic fold and transcritical bifurcations appear once more.

VI. Dynamics of the Poincaré Map

This section shows how switching time bifurcations affect the Poincaré map F which describes the circuit transient dynamics [5], [15]. F advances the system state $y(0)$ at time zero by one period T so that $F(y(0)) = y(T)$. F is computed by successive integration of the circuits with one thyristor on and with no thyristors on encountered during the cycle. If a periodic orbit of period T passes through $y(0)$ at time zero, then F has a fixed point $y(0)$ corresponding to the periodic orbit.

The fold switching time bifurcations of Section IV cause the switching time to vary discontinuously. Near a switching time bifurcation, these switching time discontinuities can cause two initially nearby trajectories to separate greatly because a portion of one trajectory occurs in a circuit with a thyristor on while the same portion of the second trajectory occurs in a circuit with a thyristor off. (Note that, in contrast to ideal diode circuits [3], the delay of thyristor switch on until there is a firing pulse typically prevents the thyristor in the second trajectory from turning on again just after it turns off.) Therefore the fold switching time bifurcations typically cause discontinuities of the Poincaré map. If the initial condition $y(0)$ is such that a switching time bifurcation occurs at one of the switching times in the cycle, then F is discontinuous at $y(0)$. We write Θ for the set of discontinuities of F. F is smooth away from Θ [3].

The Poincaré map F is not one to one. We can see this by computing the Poincaré map for a segment of a circular disk of initial conditions of radius 10 (cf. Fig. 7). The overlapping portion of Fig. 7 indicates a non invertible map, and numerical experiments confirm this. For example, the initial conditions (3.0,8.19°) and (3.2,-31.01°) map onto the same point. Here it is convenient to specify initial conditions $y(0)$ in polar coordinates (r, θ).

To avoid the region of misfires, we restrict the domain of F to $\{-89° \leq \theta \leq 89°\}$. Computer experiments show that $\{-89° \leq \theta \leq 89°\}$ is positively invariant under F. The Appendix shows that there is a compact positively invariant set Ω such that every initial condition in $\{-89° \leq \theta \leq 89°\}$ tends to Ω. Computing $\bigcap_{i=1}^{n} F^i(\Omega)$ yields all the attractors inside $\{-89° \leq \theta \leq 89°\}$. After 30 iterates, $\bigcap_{i=1}^{30} F^i(\Omega)$ becomes the two fixed points $y_1 = (1.06, -58.18°)$ and $y_2 = (19.92, 58.45°)$ which correspond to orbits of period T and are not in Θ. It can be shown [4], [3] that all periodic orbits of the thyristor controlled reactor circuit with $y(0) \notin \Theta$ are asymptotically stable. Thus we have demonstrated multiple attractors for the thyristor controlled reactor circuit. This contrasts with the unique attractors of suitably resistive ideal diode circuits [3].

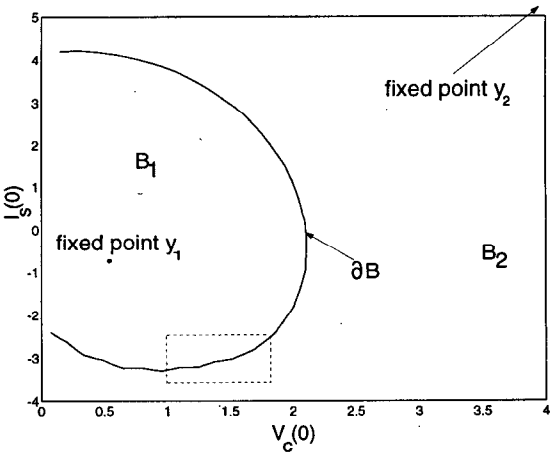

Fig. 8. Basin boundary separating basins of fixed points.

VII. Basins of Attraction

The basin boundary ∂B separating the basins of attraction of the two fixed points y_1 and y_2 is of interest because it interacts with the set of Poincaré map discontinuities Θ. Fig. 8 shows the basins of attraction B_1, B_2 of each fixed point and the basin boundary ∂B (∂B is formally defined as the intersection of the closures of B_1 and B_2). ∂B was computed by taking a fine grid of initial conditions and noting which of the two fixed points they converged to under repeated application of the Poincaré map F. The basin boundary interacts with Θ inside the dotted rectangle of Fig. 8 which is shown enlarged in Fig. 9.

Fig. 9(a) shows the fine structure of Θ only. Θ is composed of 3 curves C_1, C_2, C_3 which were computed by a continuation method. Initial conditions on C_1 yield switching time bifurcations in the first half cycle as shown in the corresponding inset of Fig. 9(a) (the inset shows the qualitative form of thyristor current $I_r(t)$ for initial conditions on C_1 and $*$ indicates a switching time bifurcation). C_2

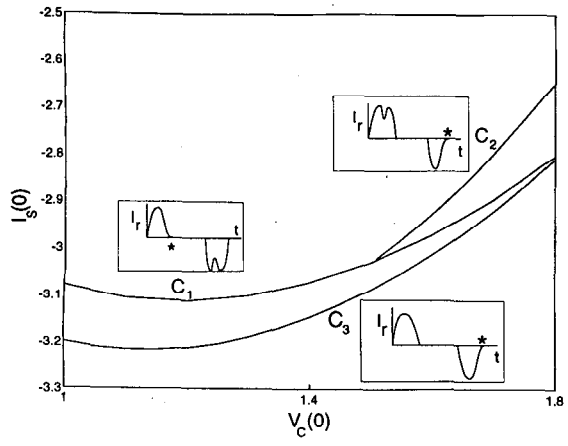

(a)

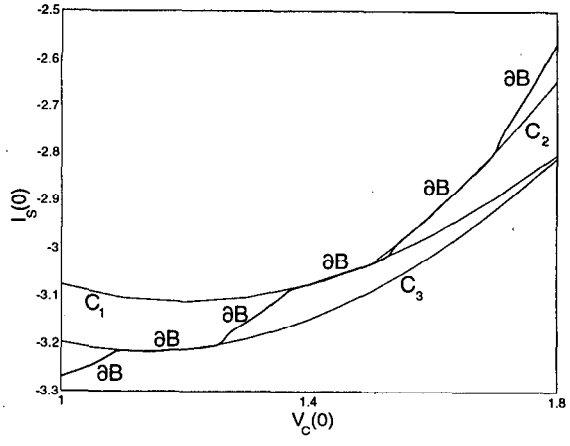

(b)

Fig. 9. (a) Detail of Poincaré map discontinuities Θ. (b) Detail of Θ and basin boundary ∂B.

and C_3 correspond to switching time bifurcations in the second half cycle as shown in the corresponding insets of Fig. 9(a).

Fig. 9(b) shows how the basin boundary ∂B intersects with Θ. Let X be the points in ∂B and Θ:

$$X = \partial B \cap \Theta.$$

X consists of initial conditions on the basin boundary which encounter a switching time bifurcation during the next cycle. The discontinuity in F caused by switching time bifurcation is the mechanism by which nearby initial conditions on either side of X tend to different fixed points under iterations of F. Numerical application of F to X suggests that initial conditions exactly on X tend to the fixed point y_2. That is, X is contained in the basin B_2. To understand this, note that in the fold switching time bifurcation in Fig. 3, the switch off time $\sigma(\lambda)$ is continuous at the switching time bifurcation when $V_c(0) = V_* \approx 5.1$ as $V_c(0)$ approaches V_* from above, but is discontinuous at V_* as $V_c(0)$ approaches V_* from below. This one sided continuity causes the points in X to tend to y_2 under iterations of F.

Let Y be the portion of the basin boundary ∂B not in X. Points of Y map to X under a repeated application of F. To show this, we computed the dynamics on Y as follows. First, we claim that F maps Y into ∂B. (Let $y(0) \in Y$, and let U be a neighborhood of $y(0)$ which intersects both B_1 and B_2 but is disjoint from Θ. F is smooth in U and $F(B_1 \cap U) \subset B_1$, $F(B_2 \cap U) \subset B_2$ imply that $F(y(0)) \in \partial B$.) Parameterizing the basin boundary ∂B by θ,

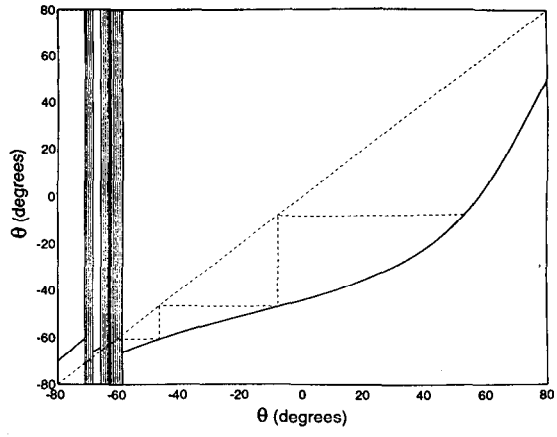

Fig. 10. Poincaré map of basin boundary ∂B.

we computed F on Y to yield the one dimensional map shown in Fig. 10 (the shaded portions correspond to X). The form of the map in Fig. 10 shows that repeated iterates of F map Y to X (one such iterate is shown).

In summary, the basin boundary ∂B consists of initial conditions which are either on X or eventually map to X. Thus the forward trajectory through every initial condition on ∂B encounters a switching time bifurcation which causes the two basins to be separated. However, there are also many initial conditions in Θ but not in ∂B whose forward trajectories encounter switching time bifurcations. The basin boundaries of conventional smooth dynamical systems contain unstable orbits such as saddles which act to separate trajectories in different basins. No such unstable orbits appear to exist in ∂B.

VIII. Conclusion

We have described switching time bifurcations of a thyristor controlled reactor circuit using fold and transcritical bifurcations of the thyristor current function f which determines the thyristor switching times. The discontinuities in the switching times greatly affect the circuit transient dynamics, causing discontinuities and noninvertible regions of the Poincaré map. The circuit exhibits two asymptotically stable periodic orbits and no unstable periodic orbits. The basin boundary separating the two basins of attraction of the two periodic orbits is composed of some of the initial conditions whose forward trajectories encounter switching time bifurcations. We conclude that switching time bifurcations in the thyristor controlled reactor circuit cause novel dynamics not present in conventional nonlinear dynamical systems. These novel dynamics are generic and should help to clarify nonlinear phenomena in other circuits with ideal thyristors.

Appendix

This appendix shows the existence of a compact positively invariant and globally attracting set for F by a combination of analytical and numerical results. F is assumed to be restricted to $\{-89° \leq \theta \leq 89°\}$.

According to [4], [8],

$$F(y(0)) = J(y(0))\, y(0) + g(u)$$

where $g(u)$ is a bounded function of u. The matrix $J(y(0))$ is the Jacobian of F if $y(0) \notin \Theta$. Choose the norms related to the circuit energy (see [3]) by

$$|y(t)|^2 = \tfrac{1}{2} C V_c(t)^2 + \tfrac{1}{2} L_s I_s(t)^2$$
$$|x(t)|^2 = \tfrac{1}{2} L_r I_r(t)^2 + \tfrac{1}{2} C V_c(t)^2 + \tfrac{1}{2} L_s I_s(t)^2$$

and write $||.||$ for the induced matrix norms. From [8], [3],

$$J(y(0)) = Pe^{A\tau_1}Q\,e^{PAQ(T/2-\tau_1)}Pe^{A\tau_2}Q\,e^{PAQ(T/2-\tau_2)}$$

where τ_1, τ_2 are the length of time each thyristor conducts and Q is the transpose of P. Using $||P|| \leq 1$ and $||Q|| = 1$ from [3],

$$||J(y(0))|| \leq ||e^{A\tau_1}||\,||e^{PAQ(T/2-\tau_1)}||\,||e^{A\tau_2}||\,||e^{PAQ(T/2-\tau_2)}||.$$

It can be checked that $||e^{A\tau_1}|| < 1$ for $\tau_1 > 0$ and that $||e^{PAQ(T/2-\tau_1)}|| < 1$ for $\tau_1 < T/2$. Therefore $||e^{A\tau_1}||\,||e^{PAQ(T/2-\tau_1)}|| < 1$ for $0 \leq \tau_1 \leq T/2$ and $\sup||J(y(0))|| < 1$. Let

$$R = \frac{2\sup|g(u)|}{1-\sup||J(y(0))||}.$$

Then $|y(0)| \geq R$ implies

$$|F(y(0))| \leq (\sup||J(y(0))||)|y(0)| + \sup|g(u)| < k|y(0)|$$

where k satisfies $(1+\sup||J(y(0))||)/2 < k < 1$. Let

$$\rho = 1 + R + \Big|\max_{|y(0)|\leq R}|F(y(0))| - R\Big|.$$

Then $|y(0)| \leq \rho$ implies $|F(y(0))| < \rho$. Since $\{-89^\circ \leq \theta \leq 89^\circ\}$ is positively invariant, the set

$$\Omega = \{\,|y(0)| \leq \rho,\ -89^\circ \leq \theta \leq 89^\circ\,\}$$

is a compact positively invariant set. Moreover since $0 < k < 1$, and $|y(0)| \geq \rho$ implies $|F(y(0))| < k|y(0)|$, every initial condition in $\{-89^\circ \leq \theta \leq 89^\circ\}$ tends to Ω. Numerical results show that $\rho = 500$ is a suitable choice.

REFERENCES

[1] L. J. Bohmann and R. H. Lasseter, "Harmonic interactions in thyristor controlled reactor circuits," *IEEE Trans. Power Delivery*, vol. 4, pp. 1919-1926, July 1989.

[2] N. Christl, P. E. Krause, R. Hedin, *et al.*, "Advanced series compensation (ASC) with thyristor controlled impedance," in *Conf. Int. Grands Réseaux Electriques*, CIGRÉ paper SC 14/37/38-05, Paris, France, 1992.

[3] I. Dobson, "Stability of ideal thyristor and diode switching circuits," *IEEE Trans. Circuits Syst. I*, vol. 42, pp. 517-529, Sept. 1995.

[4] I. Dobson, S. G. Jalali, and R. Rajaraman, "Damping and resonance in a high power switching circuit," *Systems and Control Theory for Power Systems*, J. H. Chow, P. V. Kokotovic, and R. J. Thomas, Eds., IMA vol. 64 in *Mathematics and Its Applications*. New York: Springer-Verlag, 1994, pp. 137-156.

[5] J. Guckenheimer and P. Holmes, *Nonlinear Oscillations, Dynamical Systems and Bifurcations of Vector Fields*. New York: Springer-Verlag, 1986.

[6] L. Gyugyi, "Power electronics in electric utilities: Static var compensators," *Proc. IEEE*, vol. 76, pp. 483-494, Apr. 1988.

[7] *Current Activity In Flexible AC Transmission Systems*, IEEE Rep. 92 TH 0465-5 PWR, Apr. 1992.

[8] S. G. Jalali, I. Dobson, R. H. Lasseter, and G. Venkataramanan, "Switching time bifurcations of a thyristor controlled reactor," *IEEE Trans. Circuits Syst. I*, vol. 43, pp. 209-218, Mar. 1996.

[9] S. G. Jalali and R. H. Lasseter, "Harmonic instabilities in advanced series compensators," *EPRI FACTS Conf.*, Boston, MA, May 1992, in *Electric Power Research Inst.*, Rep. TR-101784.

[10] P. Kundur, *Power System Control and Stability*. New York: McGraw-Hill, 1994.

[11] E. Larsen, C. Bowler, B. Damsky, and S. Nilsson, "Benefits of thyristor controlled series compensation," in *Conf. Int. Grands Réseaux Electriques*, CIGRÉ paper SC14/37/38-04, Paris, France, 1992.

[12] T. J. E. Miller, Ed. *Reactive Power Control in Electric Systems*. New York: Wiley, 1982.

[13] R. Rajaraman, I. Dobson, S. G. Jalali, "Nonlinear dynamics and switching time bifurcations of a thyristor controlled reactor," in *Int. Symp. Circuits Syst.*, Chicago IL, May 1993, pp. 2180-2183.

[14] R. Rajaraman, "Damping of subsynchronous resonance and nonlinear dynamics in thyristor switching circuits," Ph.D. dissertation, Univ. Wisconsin-Madison, 1996.

[15] J. M. T. Thompson and H. B. Stewart, *Nonlinear Dynamics and Chaos: Geometrical Methods for Scientists and Engineers*. London, U.K.: Wiley, 1986, reprinted 1987.

Chaotic Behavior and Synchronization Phenomena in a Novel Chaotic Transistors Circuit

Cong-Kha Pham, Makoto Korehisa, and Mamoru Tanaka

***Abstract*— In this brief, chaotic behavior and synchronization phenomena which occur in a novel Chaotic Transistors circuit with *high speed operation* are described. The most important point in this brief is to *change* a nonlinear transfer characteristic of a MOS inverter to a nonlinearity generating a chaos. The proposed circuit includes a looped MOS inverter having a pull-up resistor serially connected to a pull-down NMOS transistor. A switched capacitor (SC) circuit having a hold capacitor and two CMOS switches is added in the loop of the circuit to operate sampling holding. The chaotic behavior has been found along with a variation of a sampling clock frequency. The synchronization phenomena is also found between two coupled Chaotic Transistors circuits. The test chip is implemented employing 2 μm CMOS technology of MOSIS service.**

I. INTRODUCTION

There are many studies on chaotic behavior in nonlinear systems in the recent decade [1]–[12]. The nonlinear feedback system such as a pulsewidth modulated (PWM) system with a difference equation generates chaos if this equation has periodic solution of each period as described in [1]. The chaotic phenomena is also found in a negative resistance LC oscillator as shown in [2] and in a two cells or three cells autonomous system of cellular neural networks which exhibits the Hopf-like bifurcation as shown in [3]. On the other hand, there are many studies on chaotic behavior based on the nonlinear differences equations or nonlinear mapping functions have been reported in [4]–[12]. The very simplest nonlinear difference equations can possess an extraordinarily rich spectrum of dynamical behavior, from stable points, through cascades of stable cycles, to a regime in which the behavior is in many respects chaotic, or indistinguishable from the sample function of a random process [4]. In [5], an example of a one-dimensional (1-D) map, also called logistic map which exhibits complicated behavior such as chaos is used for analyzing experimentally the chaotic dynamics and bifurcations of circuits and systems. Recently, a neuron model with an N shaped 1-D mapping function which exhibits chaotic behavior called chaotic neuron [6]–[11] has been investigated and can be implemented with

Manuscript received January 23, 1995; revised February 12, 1996. This paper was recommended by Associate Editor M. P. Kennedy.

C.-K. Pham is with the Faculty of Business Administration and Information Science, Department of Information Science, Tokyo University of Information Sciences, Chiba, 256 Japan.

M. Korehisa and M. Tanaka are with the Faculty of Science and Technology, Department of Electrical and Electronic Engineering, Sophia University, Tokyo, 102 Japan.

Publisher Item Identifier S 1057-7122(96)08343-2.